



Research Signpost
37/661 (2), Fort P.O.
Trivandrum-695 023
Kerala, India

Remote Sensing Optical Observations of Vegetation Properties, 2010: 131-163
ISBN: 978-81-308-0421-7 Editors: Fabio Maselli, Massimo Menenti and Pietro Alessandro Brivio

6. Analysis of vegetation response to climate variability using extended time series of multispectral satellite images

M. Menenti^{1,3}, L. Jia², S. Azzali², G. Roerink²,
M. González-Loyarte⁴, S. Leguizamón⁵ and W. Verhoef⁶

¹*Department of Earth Observation, Delft University of Technology, The Netherlands*

²*Wageningen University and Research Centre, The Netherlands;* ³*Institute for Agricultural and Forest Systems CNR, Ercolano, Italy;* ⁴*Consejo Nacional de Investigación Científica y Tecnológica, Mendoza Argentina;* ⁵*Universidad de Mendoza, Mendoza, Argentina;* ⁶*National Aerospace Laboratory Emmeloord, The Netherlands*

Abstract. Satellite observations of the terrestrial biosphere cover a period of time sufficiently extended to allow the calculation of reliable climatologies. The latter is particularly relevant for studies of vegetation response to climate variability. This chapter reviews studies done by the authors since the late 80-s on the use of time series analysis techniques to extract concise information from extended time series of large area multispectral satellite data. Two basic methods have been used: the Fast Fourier Transform, especially in the earlier studies, and Harmonic Analysis in more recent work. Since the first studies, work has been relying on the global radiometric data collected by AVHRR and later on MODIS, as well as it has been performed in different continents. The applications supported by published results are:

Correspondence/Reprint request: Dr. Massimo Menenti, Department of Earth Observation, Delft University of Technology, The Netherlands. E-mail: M.Menenti@tudelft.nl

- a) the identification and mapping of zones characterized by a similar response of terrestrial vegetation to environmental forcing;
- b) the determination and characterization of terrestrial vegetation response to climate variability over any period of time covered by available time series of satellite data;
- c) early warning of anomalies detected during the growth of terrestrial vegetation by using indicators of photosynthetic activity such as NDVI and fAPAR.

Introduction

Climate variability has a very significant impact on the evolution of vegetation cover. This relationship can be analyzed using observations of climatic forcing factors and of vegetation response, applying, in both cases, global data sets i.e. re-analysis data obtained by atmospheric models and spectro-radiometric data collected by satellites. Available re-analysis data span a period of more than 40 years while the spectro-radiometric satellite data more than 25 years and these time series are sufficiently long to carry out studies of climatological relevance. Early examples of time series analysis of satellite data to study terrestrial vegetation and its response to climate variability were published in the early 90-s [1,2].

The study of vegetation cover types, phenology and climate conditions has been successful through the application of NOAA-AVHRR NDVI imagery at regional scale [3-7]. Potter and Brooks [8] explained 70-80% of the spatial variability found in the NDVI seasonal extremes for different plant functional types by applying climate indices calculated with temperature and rainfall data. Henricksen and Durkin [9] demonstrated that the start and the end of the growing season in Ethiopia, assessed with NDVI images, were strongly related to a moisture index. Additionally, Hielkema et al. [10] calculated that the integrals of NDVI for each growing season were closely correlated with rainfall in the Sudanese savanna. A strong linear relationship was also found between NDVI and the annual rainfall in the range of 150-1000 mm in the western Sahel [11]. More recently, Anyamba and Tucker [12] applied the analysis of NDVI data to derive information on the Sahelian vegetation growth dynamics in response to rainfall variability during the period 1981-2003. They consistently detected drought and 'wetter' conditions in agreement with the region-wide trends in rainfall events. Justice et al. [13] found a general relationship between rainfall estimates from Meteosat and NOAA-AVHRR NDVI data wherein the time lag between rainfall events and NDVI was particularly evident when rainfall was the limiting factor for vegetation growth. Different authors demonstrated the usefulness of applying NOAA-AVHRR NDVI to detect the effect of droughts in Ethiopia [9,14] and in Sahel [15,16]. Recently, NOAA-AVHRR NDVI series have been applied to study

the inter-annual variability induced by the ENSO events [17-20]. Liu and Negrón Juárez [17] could calculate large anomalies of NDVI and ENSO indices for drought forecast in Northeastern Brazil. The anomalies were spotted four months in advance and had 68% of success rate.

The novelty of the methodology here described is the simultaneous characterization of three aspects: spatial and temporal variability of vegetation cover as well as its dynamic response to forcing factors. Such result is obtained thanks to the analysis of time series for each image element (pixel). Analyses of the relationship between climate variability and photosynthetic activity were performed in Africa [21,22], South America [21,23, 28], Europe [24,25,26] and China [27]. The impact of rainfall anomalies on foliar phenology, in terms of timing (phase) and intensity of greenness, was studied by using Fourier series to fit a time series of NDVI observations.

Such approach involved the study of three different but related aspects:

1. characterization and mapping of climate-soil-vegetation complexes or isogrowth zones [2,21,22];
2. quantitative analysis of the response of foliar phenology to climate variability [24,25,26,28];
3. early detection of drought-related anomalies in the growth of vegetation [27].

Mapping climate-soil-vegetation complexes

The objective is to characterize and map areas wherein vegetation development is similar due to a unique combination of climate, soil and association of vegetation species. For those particular areas the concise notation of “isogrowth zones” has been then used. Isogrowth zones are mapped by applying classical numerical classification algorithms to images of Fourier coefficients obtained by modeling the time series of NDVI observations for each pixel. The results of the classification are then analyzed and documented by correlation with both soil and vegetation maps as well as with climate data. In all the performed studies a clear correlation was observed between isogrowth zones and a measure of aridity such as the Budyko ratio.

Vegetation phenology and climate variability

Climate forcing is accounted by using observations of net radiation and precipitation, more precisely their ratio (Budyko index), which is a measure of excess radiant energy at the land surface relative to available water and, therefore, of drought hazard [29-31]. The response of vegetation as characterized by photosynthetic activity is obtained by estimates of the fraction

of Absorbed Photosynthetically Active Radiation (fAPAR). These estimates are obtained with multispectral radiometric data collected by a series of imaging radiometers installed on satellites operated from 1979 onwards. The results summarized in this review were obtained with data collected from the Advanced Very High Resolution Radiometer (AVHRR) and from the Moderate Resolution Imaging Spectroradiometer (MODIS).

Early detection of drought – related anomalies

The analysis of annual time series of NDVI observations suggested [27] that the deviations of current year observations from the reference (average) year can be detected in the earlier stages of the growing season, providing crucial information to predict the peak magnitude of anomalies in advance on the actual occurrence of a drought spell.

Modeling of NDVI time series by means of Fourier series or with other techniques can be used to fill missing data in the time series, including those ones due to clouds, to remove image noise and to extrapolate data in time by using a moving window during the calculation of the Fourier transform. Even though the prediction accuracy increases with decreasing lead time, an early warning of an anomaly during the vegetation growth season is very useful for the estimation of drought impacts, particularly in agriculture.

1. Approach

1.1. Fast Fourier Transform and Harmonic Analysis

The Fast Fourier Transform (FFT) algorithm, applied in this study, allows to decompose the NDVI series for each pixel in an average signal plus $N/2$ sinusoidal components, with N being the length of the time series expressed as the number of images [21]. The average signal is the mean NDVI value for the whole time series of observations and the periodic (sinusoidal) components are characterized by amplitude and phase. All of them, mean NDVI, and amplitude and phase for each period, are called in this paper Fourier coefficients.

Amplitude and phase are associated with a given period, e.g. 12 and 6 months in our analysis. The amplitude value represents a measurement of the maximum variability of NDVI at a given period, and phase is the timelag of this maximum in relation to the initial point of the series. The decomposition of a complex time series of NDVI images into simpler periodic signals allows to understand the relative weight of different periodic climate processes like rainfall and temperature on vegetation complexes [22] as well as foliar seasonality [32] in Southern Africa.

The Harmonic Analysis algorithm allows the use of irregularly spaced observations and the frequency of periodic functions can be selected by the user. The method has been described by Menenti et al. [1,2,33], Verhoef et al. [25], Azzali and Menenti [21,22], Roerink et al. [33,34]. This algorithm consists of a curve-fitting procedure based on harmonic components and it can be considered a generalization of the maximum value compositing normally applied to generate NDVI data products. In practice, time series of NDVI contain cloud – contaminated observations even after the classical maximum value compositing algorithm is applied [24].

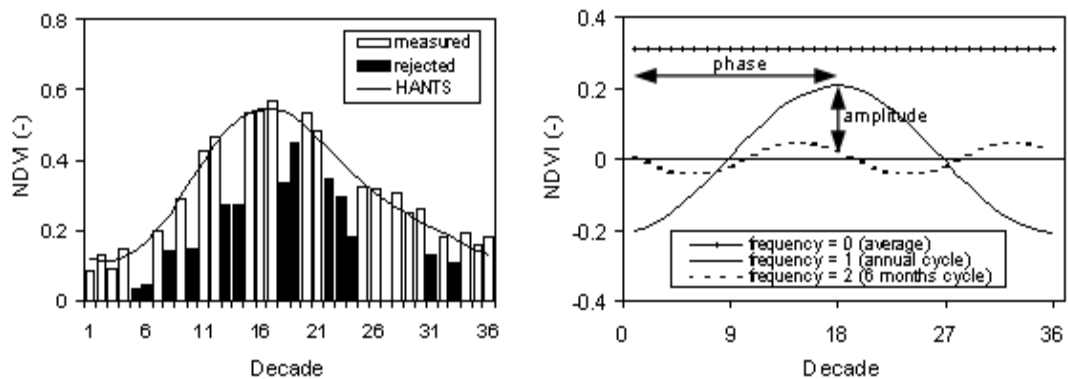


Figure 1. Schematic description of the HANTS algorithm: (left) identification and removal of outliers and (right) resulting Fourier coefficients of the filtered time series.

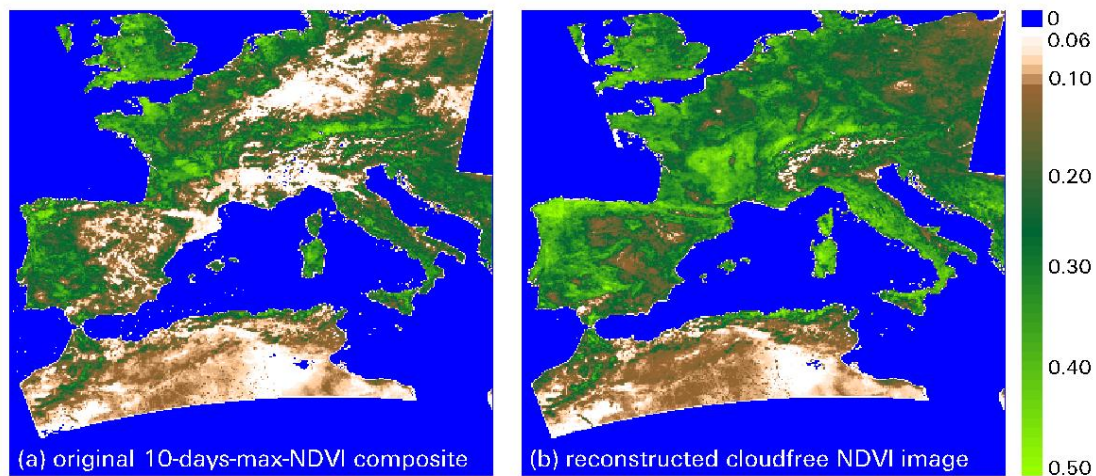


Figure 2. Weekly composite NDVI image of Europe and North Africa: (left) original image with standard radiometric corrections and cloud flagging and (right) after removal of cloud contaminated observations and gap-filling using the HANTS algorithm [24, 26].

The Harmonic Analysis of NDVI Time Series (HANTS) algorithm allows the user to select dominant frequencies, e.g. on the basis of a preliminary FFT analysis and applies a least squares fitting procedure based on the selected harmonic components.

Filters may be applied in order to identify and remove anomalous observations (Fig. 1), due to e.g. clouds.

As a consequence, this procedure yields time series of irregularly spaced observations, which may be different for each pixel. Although this result comes at a price in terms of processing time, it allows to maximize the number of valid observations and, therefore, of information extracted from the time series. Once the valid observations are fitted by the final Fourier series, the latter can be used to fill gaps in the observations for each final to obtain a cloud-free image of the observed area (Fig. 2).

1.2. Large area mapping of climate-soil-vegetation complexes

Isogrowth – zones

The most obvious feature of large area vegetation processes is the phenology of land cover. Even without a precise definition of measurable parameters to characterize it, land cover dynamics is an integrated response to a variety of climate, biotic, physiographic and anthropological processes [35-40]. It is this integrating property of land cover dynamics that provides the key to the description and understanding of large area ecosystems [41-45].

In this context, temporal records of vegetation properties has been already applied since the '70s to characterize terrestrial ecosystems and to understand the weather and climate influences on vegetation [46,47].

Particularly, phenology is an essential part of the overall adaptive strategy of vegetation to the environment and is an extremely sensitive response indicator to climate, soil and land management. Consequently, the ability to investigate the timing of vegetation development (green foliage duration and intensity) and its senescence with frequent and consistent observations is a crucial tool for the study of natural and agricultural environments. Satellite remote sensing has provided a way to measure and monitor phytophenology at the regional as well as at the global scale [47]. Many examples of large-area classification of vegetation at different phenological stages using NOAA AVHRR NDVI data can be found in literature [5, 48-51]. Since multi-temporal satellite observations are already available for long time spans the challenge has been to develop an efficient approach to extract concise information from large amounts of data. In practice, the use of time series techniques has

provided a significant answer to it by giving a parsimonious description of vegetation phenology [1,2, 52-56].

Classification algorithms

Both the FFT and the HANTS algorithms provide images of the Fourier coefficients, i.e. pixelwise values of amplitude and phase for all frequencies considered, which result in maps of the quantitative measurements of vegetation phenology. Such maps supply measures of the vegetation response to environmental processes, which enable the identification of “isogrowth zones”.

To this end numerical classification procedures widely used in combination with spectral attributes of vegetation, can be applied. It is not straightforward, however, to define a-priori large area “isogrowth zones”, and supervised (hard) classification algorithms cannot be applied. Consequently, unsupervised and fuzzy classification techniques have, in this context, a significant potential. As results of several alternate classification strategies and algorithms two solutions have emerged:

- a) apply, first, an unsupervised classification algorithm [57] to define classes and form alternate sets of signatures; the second step consists in a supervised classification procedure supported by performance indicators [58,59] which help to select the best definition of classes and associated signatures;
- b) apply, first, an unsupervised classification algorithm, as above, followed by a fuzzy classification procedure; this strategy assigns membership values to each pixel for all classes considered, rather than assigning each pixel to a class only.

Both strategy (a) and (b) require an ex-post analysis on the basis of ancillary information selected from soil and vegetation maps to understand what each class actually means. The climate-soil-vegetation complexes or “isogrowth zones” can be then be understood in terms of a combination of known attributes [60,22].

1.3. Response of vegetation phenology to climate variability

Work done towards mapping the “isogrowth zones” has documented a close relationship between vegetation type and aridity, which was measured by using the Budyko ratio. The next question is whether a similar relationship exists between temporal patterns or, in other words, whether the response of

vegetation phenology, measured by time series of NDVI (or fAPAR) observations, can be related to climate forcing, measured by time series of Budyko ratio.

For this purpose, time series of AVHRR and MODIS NDVI as well as fAPAR data [24, 61] have been applied to characterize vegetation phenology across a range of temporal and spatial resolutions. In practice to obtain time series of Budyko ratio measurements (ratio of net radiation to precipitation), the re-analysis datasets generated by ECMWF and NCEP have been applied at a spatial resolution significantly lower than that one of the satellite data. We assume that the latter describe the effect of spatial heterogeneity (soils, physiography and land management) within the larger grid cell for which re-analysis data are available.

The data generated by atmospheric models have a spatial resolution (40 km for ECMWF, 200 km for NCEP) much lower than the satellite data (1-4 km).

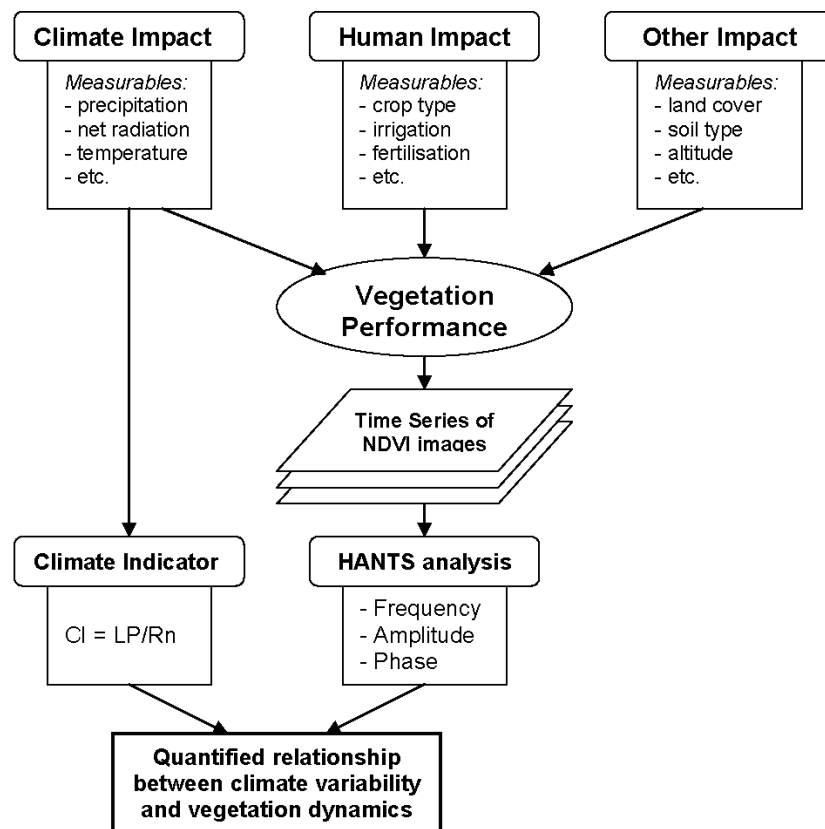


Figure 3. Schematic description of the approach proposed in this paper to study the response of terrestrial vegetation to climate variability; CI is the ratio of precipitation times the latent heat of evaporation to net radiation.

Daily values of net radiation and precipitation have been integrated over time to obtain a Budyko ratio dataset with the same temporal resolution of the satellite NDVI and fAPAR data. The latter were extracted respectively from the 30-days AVHRR and 8-days MODIS composite images. Because of the relevant difference in the grid spatial resolution between the data related to climate forcing (40-200 km.) and those of vegetation response (1 - 4 km.), we had to assume that, for a large area, climate forcing parameters are known and constant. On the other hand, the vegetation response shows, in the same large area, wide ranges of spatial variability when using higher resolution satellite data.

Menenti et al. [2] selected, for earlier studies, the Normalized Difference Vegetation Index (NDVI) instead of fAPAR.

Roerink et al. and Bolle et al. [32, 24] addressed the study of the vegetation phenological response to drought (measured by the time series of the Budyko ratio) by looking at both spatial and temporal correlation of Fourier coefficients and selecting the amplitudes of dominant components, with the help of yearly average value of the Budyko ratio.

Furthermore, the above mentioned studies have been extended to the analysis of inter-annual variability of vegetation phenology by evaluating the ratio of changes in the Fourier coefficients to the corresponding changes in the Budyko ratio values. Figure 3 shows the schematic description of the approach here applied to study the response of terrestrial vegetation to climate variability.

1.4. Early detection of anomalies in vegetation conditions

Azzali (1998, personal communication) applied the HANTS algorithm to a 10 years NDVI dataset to detect anomalies in maize production within agricultural areas in three South- African districts. By using the technique of a moving window for a 2 years time-span, the results provided useful information on the influence of the rainfall amount on the temporal dynamic of maize growth and on its yield variation.

Jia and Bastiaanssen [62] further progressed in this direction building upon previous results, i.e. studying stable spatial patterns of vegetation type and average aridity conditions (sect. 1.2) as well as the steady state yearly patterns of phenology and drought (sect. 1.3). The authors focused on the use of time series analysis to model and predict observations and on the early detection of drought-related anomalies in foliar phenology.

The trends of the vegetation response can provide a measure of drought impact as well as of drought dynamics. Knowledge of these trends is essential

for short term predictions of biomass production and in the assessment of drought impact on crop yield as well as on the vitality of natural ecosystems.

For this purpose, several satellite data products have been applied for monitoring photosynthetic activity (e.g. the MODIS fraction of Absorbed Photosynthetic Active Radiation - fAPAR - data product, the Land Surface Temperature, vegetation indices, etc.) in order to calculate the response of vegetation productivity (agriculture and forest) to drought.

Given a multi-annual time series of observations, e.g. 8-days MODIS fAPAR, the Fourier analysis is performed and the result is a gap-filled, noise-filtered time series for each year of the data set and for the average (reference) year. The occurrence and magnitude of drought-related anomalies, i.e. lower than average fAPAR and concurrent higher than average Budyko ratio, are evaluated at first. Then the model thus obtained of the yearly time series is applied to extrapolate in time the observations past the moment when the earliest anomaly is observed (DOY 121 in Fig. 4), i.e. beyond the moment when a lower than average fAPAR is first detected. (Fig. 4). The example shown in Fig. 4 clarifies how the predicted time series provides an early estimate of the maximum value of the anomaly, which in the example (Fig. 4) occurs on DOY 185.

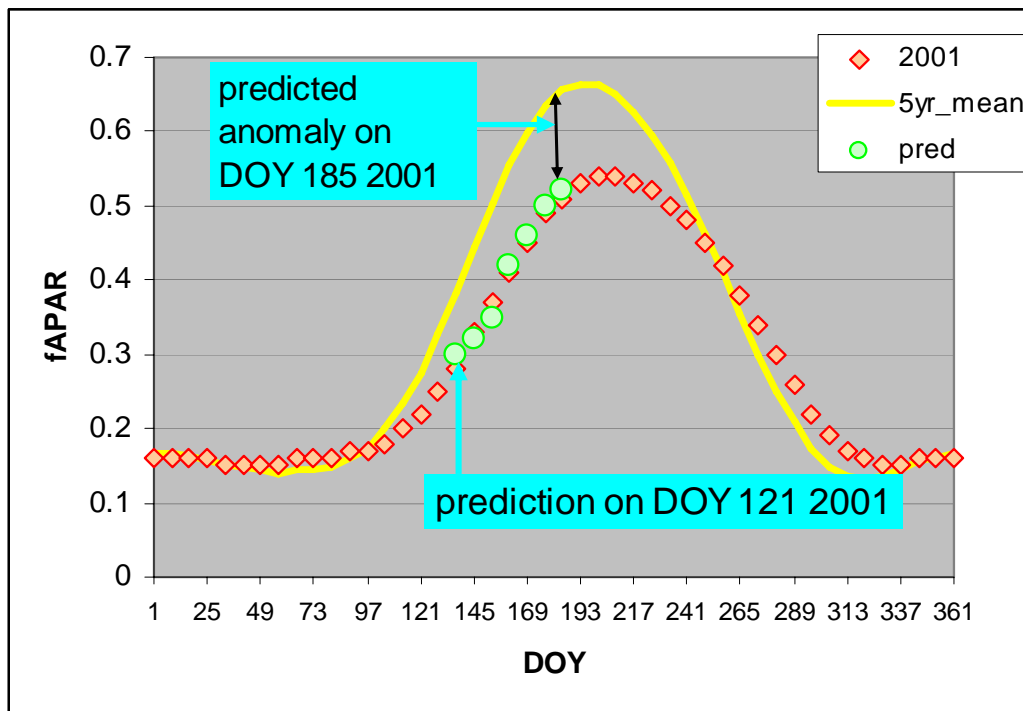


Figure 4. Modeling fAPAR time series using Fourier analysis: observations for 2001 are modeled (squares) and compared with the average year for the period 2001 – 2005 (continuous line); on DOY 121 the modeled time series over the previous 12 months is used to predict the peak anomaly on DOY 185.

This approach can be further explored by using several alternate methods (Fourier series, wavelets, Markov chains, etc.) to model the time series of observations for each individual pixel and to obtain maps of observed and predicted anomalies and of their magnitude.

2. Methods

2.1. The Fast Fourier transform and harmonic analysis

For general information on Fourier series, Fourier transform and its applications in earth sciences the reader is referred to [63-66].

A time series of NDVI or fAPAR images will be indicated as $I(x,y,t)$, where x is pixel number or longitude, y is line number or latitude and t is time in dekades (10 days) or days. $I(x,y,t)$ can be expressed as a linear combination of elementary periodic functions:

$$I(x, y, t) = \sum_{n=1}^N A(x, y)_n \exp i[w_n t - g(x, y)_n] \quad (1)$$

where w_n is frequency, A is amplitude and g is phase angle; the frequency is related to the period P_n as $w_n = 2\pi / P_n$. The maps $A(x,y)_n$ and $g(x,y)_n$ for the dominant terms in Eq.(1) represent, in a very concise manner, the information contained in the time series of image data $I(x,y,t)$.

The Fast Fourier Transform (FFT) algorithm

A time series of equidistant data points of length N can be represented by a vector I of dimension N . The Fourier transform consists of finding the amplitude vector a , such that:

$$I = U a \quad (2)$$

Where U is a $N \times N$ matrix, which contains complex numbers u on the unit circle in the complex plane. The matrix U can be organized in such a way that each element $u_{r,k}$ is given by:

$$u_{r,k} = \exp \left[2\pi (r-1)(k-1) \frac{i}{N} \right] \quad (3)$$

Where r respectively k are the row respectively column number, and $i = (-1)^{1/2}$ the imaginary unit number. By multiplying the data vector I by the complex conjugate of U , U^* we obtain:

$$U^* I = U^* U a \quad (4)$$

and finally:

$$a = [U^* U]^{-1} U^* I \quad (5)$$

Since in the special case of the Fourier transform the matrix U is square and U^*U is diagonal and equal to $N\mathbf{I}$, where \mathbf{I} is the identity matrix, the solution, in this case, is:

$$a = \left(\frac{1}{N} \right) U^* I \quad (6)$$

The mixed radix FFT algorithm implemented and applied for the investigations described in this Chapter is very fast because it calculates the matrix – vector product very efficiently by breaking it up in FFT-s of smaller dimensions. This is especially effective when N can be factored into many small (radix) numbers. In the current implementation of the algorithm, the supported radix numbers are 2,3,4 and 5, which allow to process time series of such lengths (number of data points) as 12, 36 or 360. The latter allows the analysis of multi-annual data at e.g. dekadic temporal resolution.

A disadvantage of the FFT is that data must be equidistant in time. Therefore, it would be worthwhile to weigh the input data in order to avoid that missing data have a too large impact on the results. In practice, this concept has been implemented as briefly described below.

The Harmonic Analysis algorithm

To assign weights to the input data the eq. (2) must be rewritten as:

$$W I = W U a \quad (7)$$

Here the matrix U does not contain complex numbers anymore, but rather the associated sine- and cosine series. In this case multiplying by the transposed of U , U^* , gives:

$$U^* W I = U^* W U a \quad (8)$$

with the solution:

$$a = [U^* W U]^{-1} U^* W I \quad (9)$$

where W is the diagonal matrix of weight factors. Because of these weight factors the matrix $U^* W U$ is not diagonal and its inverse must be calculated in order to find the amplitudes.

This algorithm is the solution of a generic weighted least squares fitting problem and therefore it can be used for a range of applications much wider than the FFT.

In the HANTS algorithm, as implemented, the matrix U has N rows and $2M+1$ columns, where M is the number of frequencies to be considered above the zero frequency, except if $M=N/2$, in which case the number of columns is equal to N .

2.2. Large area mapping of climate-soil-vegetation complexes

Isogrowth – zones

The areas wherein the phenology of terrestrial vegetation is similar were mapped according to the following procedure:

- a) a multi-annual data set was set up using 9 years monthly NDVI data - from August 1981 through July 1990- which was extracted from the archive created and maintained by the Global Inventory Monitoring and Modeling Systems (GIMMS) team at NASA/GSFC. These images consisted of the Global Area Coverage data re-projected to an equal area projection and re-sampled to obtain a 7.6 km x 7.6 km spatial resolution. Such monthly composites were produced, first, by screening cloud-contaminated observations through the application of Thermal Infrared Radiance in the AVHRR Channel 5 and then by searching for maximum NDVI within each month [67]. In particular, the 10 years time series were constructed with radiometric data collected within three different AVHRR sensors and calibrated with a procedure which removed the sensor-related artifacts and trends [68].
- b) The FFT mixed radix algorithm (described above) was applied to the time series of 108 monthly images. The images of mean NDVI and of the amplitudes of the 6 months, 1 year, 4.5 and 9 years components were retained for further analyses.
- c) Such selected images provided concise measurements of foliar phenology and were used as attributes in the identification of homogeneous zones with the numeric classification procedures described below.

Classification algorithms

The mapping of isogrowth zones [58,60,21,22] has been performed through the following steps:

1. The most significant attributes were selected using a measure of separability (signature divergence);
2. An unsupervised classification algorithm was applied to form alternate class definitions;
3. Several alternate classification rules were applied;
4. A measure of classification performance (IP) was created in order to compare the relatively large number of alternate classification procedures generated by the combinations of (a), (b) and (c). This indicator is based on normalized measures of reliability, separability and accuracy of the classification.
5. The highest value of IP leads to the best classification procedure.

The isogrowth zones, i.e. the classes obtained by numeric unsupervised classification procedures, need to be understood by using ancillary information on soils, climate and vegetation type. Long term averages of net radiation and precipitation were used to calculate maps of the mean Budyko ratio.

The challenge with mapping isogrowth zones using Fourier coefficients as attributes is that classes cannot be defined beforehand. An alternate solution was explored by applying a fuzzy classification (FCM) algorithm, specifically a fuzzy c-means (FCM) algorithm [69-71]. This method is a generalization of the hard c-means clustering algorithm: instead of assigning each pixel to a single class, it computes a measure of class membership for each pixel and for all classes. For this purpose, an initial set of classes is needed. The algorithm generates both a map where each pixel is assigned to the class with the highest membership and one membership map for each class and all pixels.

The membership was evaluated as:

$$m_{ij} = \frac{d_{ij}^{-2(\varphi-1)}}{\sum_{j=1}^M d_{ij}^{-2(\varphi-1)}} \quad i = 1, \dots, N; j = 1, \dots, M; M < N \quad (10)$$

where: m_{ij} = membership of pixel i for class j ; d_{ij} = distance of pixel i from centroid of class j ; φ = fuzziness exponent in the domain $(0, \infty)$; $\varphi = 1$ gives a hard classification, $\varphi = \infty$ gives uniform membership for all classes.

The obtained maps revealed that when pixels have a large membership value for a single class and much lower values for the remaining classes, a feasible definition of classes is achieved. On the contrary, occurrences of rather uniform membership values suggest that class definition is more uncertain.

2.3. Response of vegetation phenology to climate variability

The data described in Sect. 2.2 were also used to characterize the sensitivity of terrestrial vegetation to climate variability [24]. The measurements of foliar phenology provided by the Fourier coefficients were applied to characterize the vegetation response to climate variability. For this purpose, both spatial and temporal analysis of the relation between foliar phenology and aridity, measured by the Budyko ratio, was carried out.

The spatial analysis was performed by correlating the maps of relevant Fourier coefficients (mean value and amplitudes of dominant components) with the map of mean Budyko ratio.

The temporal analysis, on the other end, was carried out by computing ratios of the inter-annual changes, such as:

$$\frac{\Delta A_n}{\Delta \left(\frac{R_n}{P} \right)} = \frac{A_n(\text{year}_l) - A_n(\text{year}_k)}{\left(\frac{R_n}{P} \right)_{\text{year}-l} - \left(\frac{R_n}{P} \right)_{\text{year}-k}} \quad (11)$$

Where R_n is net radiation, P is precipitation, year_l and year_k are any paired years in the data set.

The correlation of spatial patterns of A_n and (R_n / P) for any given year k yields relationships of the kind:

$$A_n = f_k \left(\frac{R_n}{P} \right) \quad (12)$$

If this analysis is repeated for each annual data set, it is possible to evaluate the response of vegetation phenology to inter-annual variability of climate:

$$\frac{\partial A_n}{\partial t} = \frac{\partial f_k}{\partial \left(\frac{R_n}{P} \right)} \frac{\partial \left(\frac{R_n}{P} \right)}{\partial t} \quad (13)$$

where the temporal derivative is computed over any two years k and l . It should be noted that Equations 10 and 12 evaluate the temporal response of vegetation phenology to the inter-annual variability of dryness applying two fundamentally different methods. Equation 12 assumes that the inter-annual variability of Fourier coefficients (amplitude in this case) is calculated as the product of the spatial dependence of A_n on (R_n / P) at constant t and at the inter-annual change in (R_n / P) . Equation 10 does not assume any spatial dependence of A_n on (R_n / P) and treats each pixel observation as independent. We will evaluate whether Equations 10 and 12 lead to the same observed response of phenology to inter-annual variability in dryness by analysing extended time series of AVHRR data.

2.4. Early detection of anomalies in vegetation conditions

Time series analysis of NDVI and fAPAR image data has also been applied to detect drought-related anomalies. This requires modeling of the annual time series at weekly resolution removing noisy and erroneous observations and filling the resulting gaps.

This first step gives a set of high quality annual time series, $I_k(x,y,t)$ as well as the time series for the average year, i.e. the time series of the mean value of $I_k(x,y,t)$ for all available observations on the same DOY over all available years:

$$\{I_1(x, y, t), \dots, I_N(x, y, t)\} \Rightarrow \bar{I}(x, y, t) \quad (14)$$

Once $\bar{I}(x,y,t)$ has been calculated, anomalies $D_k(x,y,t)$ are defined as:

$$D_k(x, y, t) = [I_k(x, y, t) - \bar{I}(x, y, t)] \quad (15)$$

This procedure gives results which are graphically plotted as shown in Figure 4. In particular, such analysis suggest that a smooth time series might be predictable by modeling a segment of the time series, from the date of the desired prediction backwards, and by predicting the time series forward by using the model thus determined.

3. Results

The results reviewed here have been achieved through several case studies summarized in Table 1 and mentioned in the Introduction.

3.1. Large area mapping of climate-soil-vegetation complexes

Through a preliminary analysis of the significance of Fourier coefficients the selection of the most significant attributes of the isogrowth zones was performed including the mean NDVI, the amplitudes of the components with periods of 9, 4.5, 1 and 0.5 years and the phase of the components with periods of 1 and 0.5 years.

Additionally, different elements and methods were chosen to construct, apply and evaluate alternate classification procedures to map the isogrowth zones such as:

- three sets of attributes;
- inclusion or exclusion by masking of ocean and inland water;
- normalization of numeric range of attributes;
- four different sets of signatures, all including 20 classes, obtained by applying unsupervised classification;
- three different clustering rules for the supervised classification step.

Table 1. Overview of case-studies on Fourier analysis of time series of AVHRR – NDVI and MODIS fAPAR.

REGION	PERIOD	SPATIAL RES	TEMPORAL RES	METHOD	DATA
Southern Africa	August 1981 – July 1990	7.6 km x 7.6 km	30 days	FFT	AVHRR-NDVI
South America	July 1982 – June 1991	7.6 km x 7.6 km	30 days	FFT, HANTS	AVHRR-NDVI
Argentina	July 1982 – June 1991	7.6 km x 7.6 km	30 days	FFT	AVHRR-NDVI
Europe	January 1995 – December 1997	1 km x 1 km	10 days	HANTS	AVHRR-NDVI
China	January 2000 – December 2006	1 km x 1 km	8 days	HANTS	MODIS-fAPAR

Table 2. Reliability, Separability, Accuracy and overall Performance Indicator, IP, for the best six classification procedures

PROCEDURE	RELIABILITY	SEPARABILITY	ACCURACY	IP
S1	0.71	1.40	0.85	0.885
S2	0.70	1.40	0.87	0.884
S6	0.65	1.395	0.92	0.884
S7	0.68	1.40	0.74	0.85
S9	0.70	1.405	0.48	0.79
S12	0.74	1.405	0.78	0.88

Southern Africa

Each combination of the above mentioned elements yields a different classification procedure. For each procedure indicators of Reliability, Separability and Accuracy were calculated and used to determine the overall classification performance indicator, IP, as described in Sect. 2.2.

A selection of the most significant procedures, i.e. having higher IP's, were finally evaluated in more detail (Table 2).

A detailed qualitative assessment of the procedures S2, S6, S7 and S12, all obtained using the maximum likelihood Bayesian decision rule, was performed by correlation with ancillary data. Although a comparably high performance was also obtained with procedure S1, the S2 was then selected in order to compare procedures based on the same decision rule.

At this stage the isogrowth zones have been mapped by numerical classification of the Fourier coefficients, but their significance needs to be understood and documented. In practice, this evaluation was then performed by overlaying each isogrowth zone with a map of the Budyko ratio, B, and the White map of African vegetation [72]. A detailed analysis of these results was presented by Azzali and Menenti [21,22], here only a brief overview of few classes is given.

The isogrowth zones obtained with the S2 procedure, correlate rather well with both the Budyko ratio (Fig. 5a) and the White vegetation map (Fig. 5b). The isoline of $B = 2$, for example, indicates rather well the transition zone between arid and semi-arid vegetation over a broad latitude range from the southern tip of Africa towards the sub-sahelian region. The matching with the White vegetation map is also rather good, especially taking into account that the White classes are a broad association of species. Additionally, the isogrowth (or isophenology) map is able to define narrower vegetation associations, revealed by looking, particularly, at the features associated with each isogrowth zone.

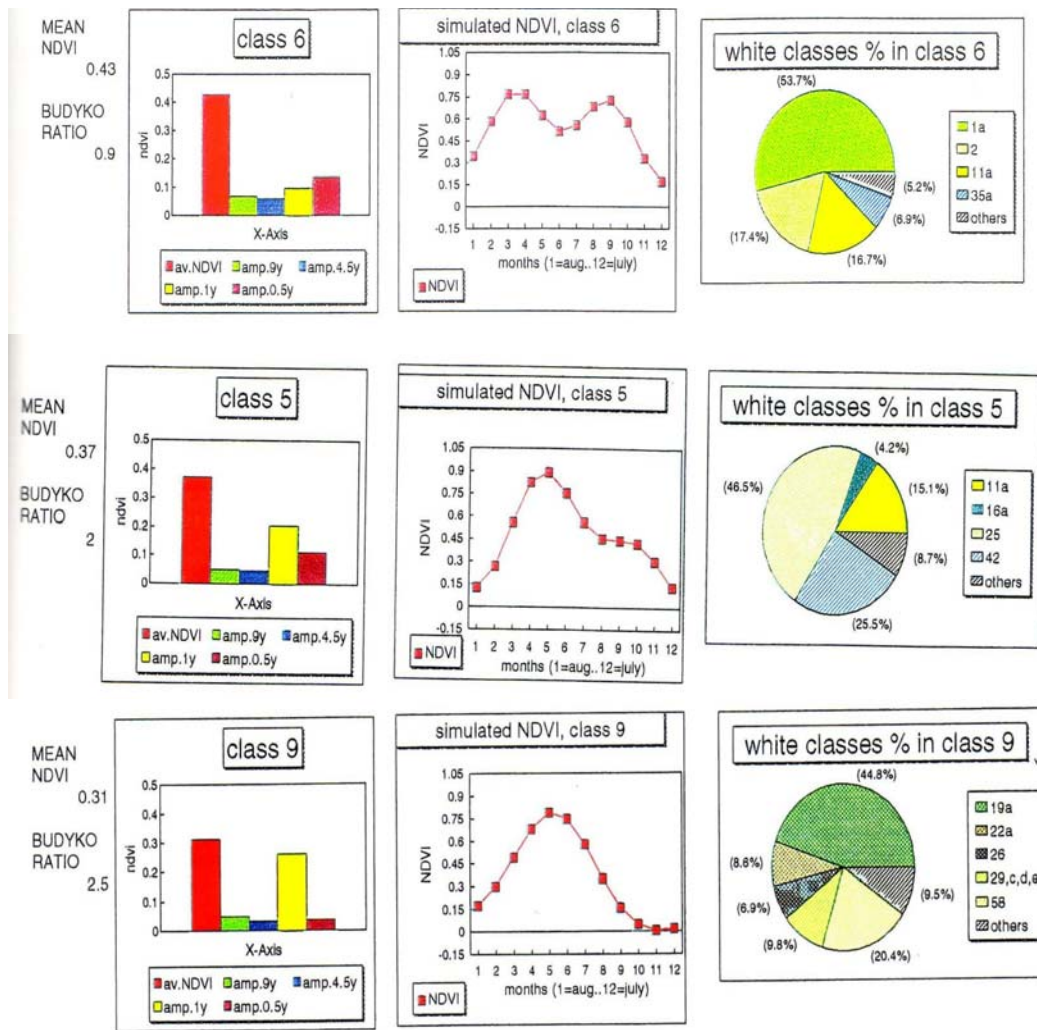


Figure 6. Legend of the map in Fig. 5 for isogrowth zones representative of the response of vegetation type to a broad range in aridity conditions; attributes of each isogrowth zone are: a) mean NDVI, b) mean B; c) Fourier spectrum; d) NDVI(t) reconstructed using the Fourier series and e) fractional abundance of White classes; classes 6,5,9.

The maps in Figure 5 include 20 isogrowth zones (classes), isolines of the Budyko ratio and White vegetation classes. Azzali and Menenti [60] described particularly the full legend of these maps with a detailed analysis of the Fourier spectra, reconstructed NDVI(t) and the relative abundance of the White classes within each one of the 20 isogrowth zones. Few examples are analyzed here to document the correlation between increasing aridity (i.e. higher values of B), Fourier spectrum (amplitudes of different periodic components), the NDVI(t) reconstructed using the Fourier series and the vegetation types as defined and mapped by White [72].

Class 6 (and the transitional class 10) have the highest mean NDVI value (0.43) in Southern Africa and Budyko values close to 1, which indicates a near equilibrium of evaporative demand (R_n) and water supply (P). Mean annual rainfall is 2000 mm. These classes are located in the dense equatorial forest areas of Central Zaire, Congo and Gabon. According to White (1983) the vegetation is classified as wetter and drier Guineo-Congolian rain forest (types 1a and 2, Fig. 5b), swamp forest (type 8), mosaics of 1a and 8, mosaics of 1a, 2 and secondary grassland (11a). Class 6 (and class 10) is the only class having a dominant 6 months component and the reconstructed NDVI(t) shows a very well defined bimodal character.

Class 5 has a mean NDVI = 0.37 and $B = 2$. Mean annual rainfall varies overall between 800 mm and 1200 mm, while it is 500 mm in Kenya where $B = 3$. The vegetation consists of Somali-Masai Acacia – Commiphora deciduous bushland and thicket (White types 42, 16a and 11a). The NDVI(t) follows the rainfall pattern with a main peak in December. The 12 months component is dominant, although the 6 months component is still significant.

Class 9 has a mean NDVI = 0.31 and $B = 2.5$. It is characterized by a seasonal rainfall (mean annual value of 700 mm) occurring during the austral summer with a peak in January. The vegetation consists of highveld grassland (type 58) and afromontane scrub forest (29c, d and e; 19a) according to White [72]. The sharp boundary between isogrowth zone 9 and zone 2 is most likely due to the higher fertility of soils within zone 9. The 12 months component is largely dominant and the amplitude is comparable with the mean NDVI. The significant amplitude values of the 9 and 4.5 years components suggest a relevant influence of the hydrological regime of the middle Limpopo river on water supply to vegetation.

South America

The FCM method described in Sect. 2.2 provides an alternate solution for mapping vegetation at a spatial scale where it is not possible to define vegetation types precisely.

Similarly to the previous case-study on Southern Africa, a subset of the Fourier coefficients, obtained with the FFT, were applied as attributes to identify homogeneous zones. The attributes included the mean NDVI, the amplitudes of the terms of the Fourier series with periods of 9, 4.5, 1 and 0.5 years and the phase values of the terms with periods of 1 and 0.5 years. The used NDVI(t) time series spanned between 1982–1991 (see Table 1).

Likewise the previous case, an unsupervised classification algorithm was used in a first step, but signatures were constructed for six classes only. Next, the membership of all pixels for the six classes was evaluated using Eq.10.

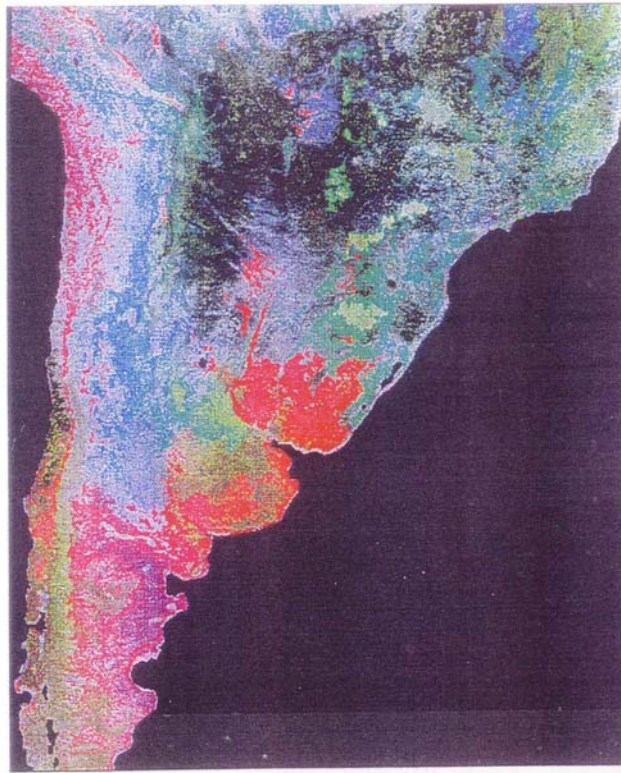


Figure 7. Map of isogrowth zones in South America showing classes 4,5 and 6 of six fuzzy classes obtained with the FCM method (see text for details); colours indicate the class of highest membership and intensity indicates the membership value

The classification results, achieved by the application of FCM, provided a set of maps: the first one where each pixel is assigned to the class for which membership is highest and M maps of the membership values of all pixels for each one of the M -classes. Part of this information can be merged into a single map (Fig. 7), where the colour indicates the class of highest membership and the colour intensity is its actual value.

The advantage of applying the FCM instead of other methods is that it provides both broader map units and information on internal variability through the membership value. This concept is well evident in Fig. 7 for the south – eastern part of Argentina where grasslands appear in magenta, showing also significant changes in intensity which indicate subtler differences in the combination of species and vegetation conditions.

3.2. Response of vegetation phenology to climate variability

The relationship between vegetation type and aridity documented by the correlation of isogrowth zones with the Budyko ratio (see e.g. Fig. 5) can be

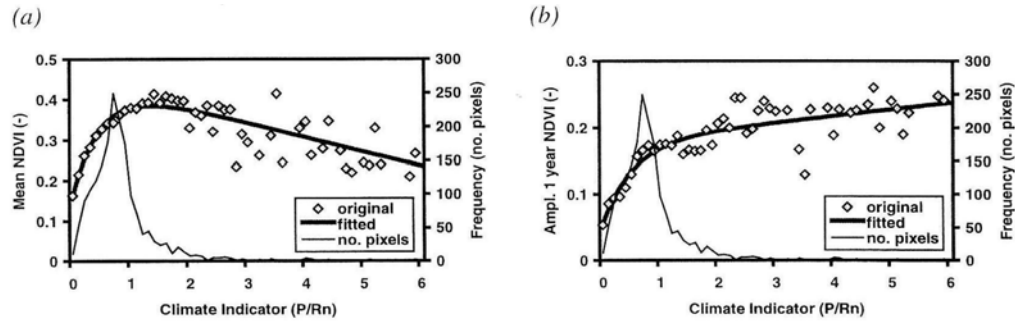


Figure 8. Mean NDVI, (a), and amplitude of the 1 year component, (b), vs. (P/R_n); Europe and North Africa, AVHRR NDVI 1996 – 1997, 10 days composites at 1 km x 1 km resolution [24,26,34].

further investigated by analysing interannual variability of vegetation phenology and of climate. This relationship is confirmed by the strong correlation of both mean NDVI and the amplitude of the 1 year component with the value of B (Fig. 8).

The values in Fig. 8 were obtained by computing, first, the Fourier transform using HANTS for two yearly time series (1996 and 1997), then, averaging the values of mean NDVI and amplitude obtained in each year for all pixels and finally sampling the resulting maps to carry out the regression analysis. The scattering in data points clearly increases with the decreasing number of pixels at increasing values of (1/B). Since climate conditions in Europe are wetter than those ones found in the previous case-studies of Austral Africa and South America, the inverse of B was here applied as the indicator of climate conditions.

The relationships in Fig. 8 have been applied to estimate the sensitivity, S , of foliar phenology to water availability by computing:

$$S = \frac{\partial A_n}{\partial (P/R_n)} \quad (16)$$

S provides a straightforward measure of sensitivity to drought. Crucial is the difference in sensitivity between the mean NDVI and the 1-year amplitude, since the value of S becomes negligible at $P/R_n \approx 1$ for mean NDVI and at $P/R_n \approx 1.5$ for the 1-year amplitude. Thus the seasonality of foliar phenology remains significant under wetter conditions than conditions affecting the average greenness of foliage. Even more interesting is the difference between the value of S obtained using data on spatial patterns at given t , i.e. using Eq. 16, or data at different times for a given pixel, i.e. using Eq. 11.

A regression analysis of those data shown in Fig. 8 was then performed to obtain the following relationship:

$$A_n = a + b(P/R_n) + c d^{P/R_n} \quad (17)$$

where the coefficients a, b, c and d depend on the order n of the periodic component under consideration.

Since the eq. 17 has been obtained with data on spatial patterns at given t , this also indicates the close relationship of spatial patterns of vegetation phenology with water availability. The sensitivity S can be then calculated by using eq. 16, given eq. 17, and obtaining the first derivative as a function of P/R_n .

Conversely, using the Eq. 11 to evaluate the sensitivity of phenology to temporal changes in water availability at a given location, it is rather evident that different functions $S(P/R_n)$ are obtained when either spatial patterns or inter-annual changes are considered (Fig. 9).

Relevant is that S becomes negligible at significantly lower values of P/R_n in the case of interannual changes (Fig. 9b) when compared with the case of spatial patterns (Fig. 9a), i.e. $P/R_n \approx 0.3$ for mean NDVI and $P/R_n \approx 0.8$ for the 1-year amplitude.

In practice, the S value provides different information when computed in the time and space domain. In the time domain it gives a measure of the phonological

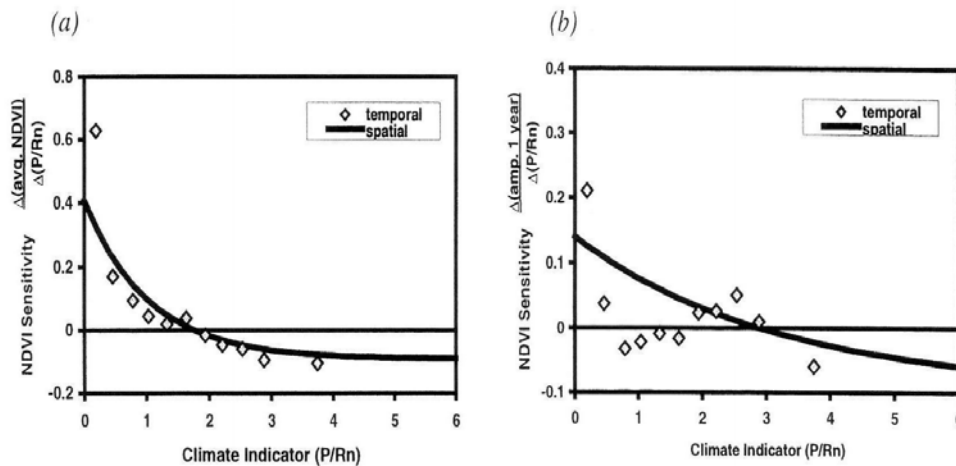


Figure 9. Sensitivity of mean NDVI, (a), and of the 1-year amplitude, (b), to interannual variability of water availability measured by the ratio P/R_n when considering spatial patterns (Eqs. 16 and 17, continuous line) or interannual changes (Eq. 11, diamonds); Europe and North Africa, AVHRR NDVI 1995, 1996 and 1997, 10 days composites at 1 km x 1 km resolution.

response of vegetation growing in an area with a given climate, i.e. at a specific value of B , showing a temporary and usually rather limited inter-annual change of B . Therefore, this S_t value is a measure of resilience of vegetation.

In the space domain, conversely, the S_s value provides a measure of differences in phenology of vegetation types growing under different climate conditions, i.e. different mean B -values. This information (S_s) may be interpreted as a measure of vulnerability of vegetation in the presence of long term changes in climate, i.e. such as to affect in a permanent way water availability at the locations considered to compute S in the space domain, S_s .

3.3. Early detection of anomalies in vegetation conditions

Timely and reliable detection of anomalies in vegetation growing conditions requires an accurate removal of anomalous observations, filling the gaps in the annual time series and a robust modeling for the valid observations.

The result by applying Eq. 14 is a set of noise-free annual time series including also the time series for the reference year obtained by averaging all available observations (for each 8 days period in different years). In practice, this data set provides a straightforward way to determine and visualize anomalies by applying Eq. 15.

A case-study [27] on the Qinghai – Tibet Plateau using MODIS fAPAR data for the period 2001 – 2005, illustrates how anomalies are detected and analysed (Fig. 10).

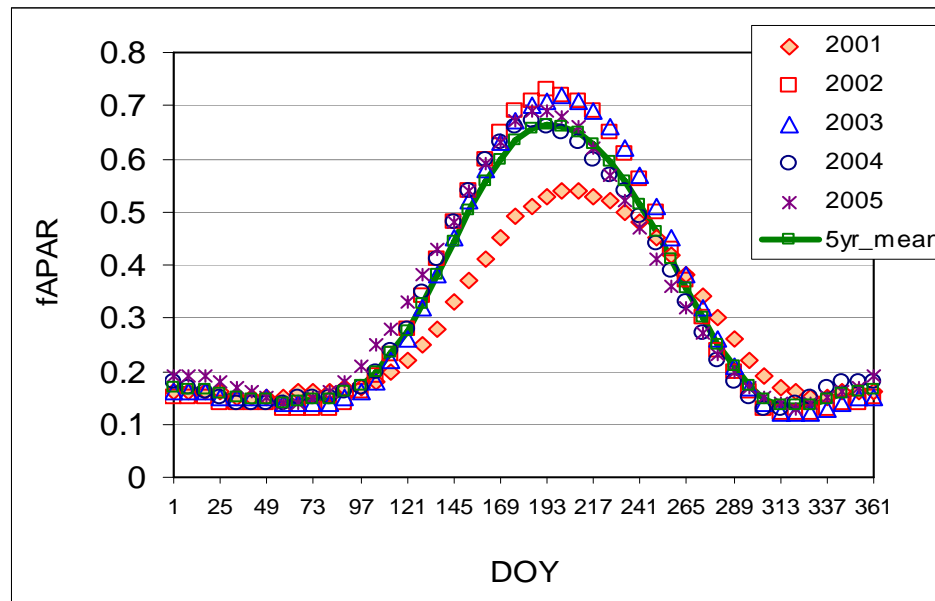


Figure 10. Observed fAPAR annual time series at a randomly selected pixel in the Tibetan Plateau; each observation is a 8-days composite; Terra / MODIS, 2001-2005 [27].

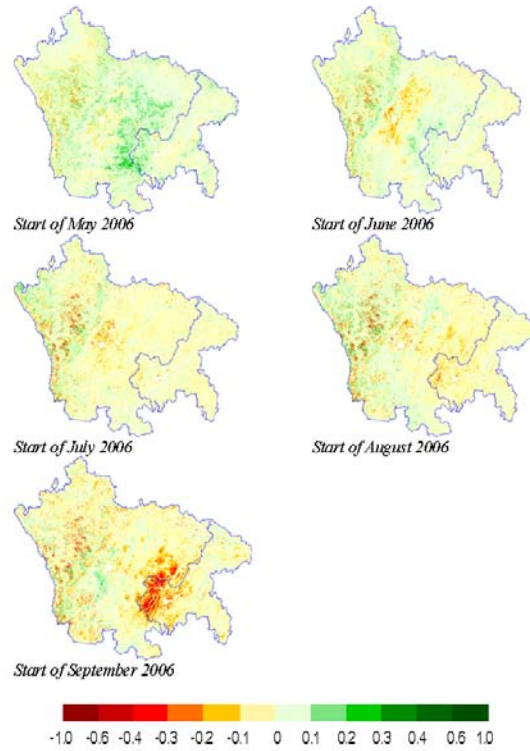


Figure 11. Anomalies in the Fraction of Absorbed Photosynthetically Active Radiation (fAPAR) observed by the MODIS satellite at 8-days intervals; anomaly is defined as difference between each 8-days value in 2006 and the corresponding average in the five year period 2001-2005; pixel size is 1 km x 1 km; Sichuan (left from the blue line) and Chongqing (right from the blue line) Provinces, China.

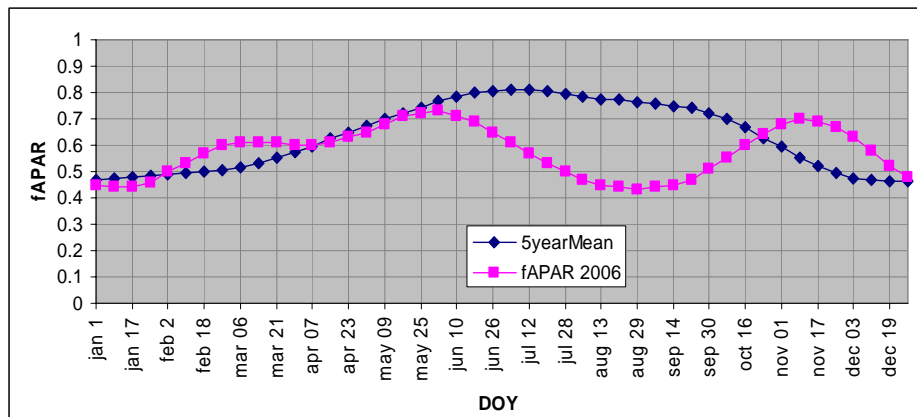


Figure 12. Fraction of Absorbed Photosynthetically Active Radiation (fAPAR) observed by the MODIS satellite at 8-days intervals for a single pixel: five years (2001 – 2005) average (blue) and 8-days observations during 2006; pixel size is 1 km x 1 km; Sichuan Province, China.

This result illustrates the basic principle of the approach: although the overall shape of the fAPAR signature remains a simple periodic function, subtle differences in timing of minimum and maximum values and in the overall yearly amplitude are noticeable. Such differences are measured by using the Fourier coefficients.

Over vast and complex regions like the Qinghai – Tibet Plateau significant differences in inter-annual variability and phenology may occur and be observed. Anomalies may occur in few areas only. Jia and Menenti [27] selected the driest (i.e. 2001) and the wettest (i.e. 2005) years within the available MODIS data. Anomalies in fAPAR were almost negligible in the southeastern portion of the Plateau and very large, i.e., in the northeastern Plateau where $\delta fAPAR = 12$ in response to $\delta (R_n / \lambda P) = 13$. This example underscores the value of the approach described here: time series of spatial data on dryness conditions and concurrent vegetation conditions are essential to observe and understand the impact of climate variability on terrestrial vegetation. The latter is particularly relevant in extensive agricultural lands: a more detailed case-study dealing with the severe 2006 drought in Sichuan and Chongqing regions of China was carried out using the approach described here.

The analysis of MODIS fAPAR observations (Fig. 11) shows that scattered anomalies occurred in the western part of the province as early as June 2nd 2006, due to irregular rainfall events, which were synchronously detected with TRMM data on the same locations.

The improvement in spatial resolution obtained with the MODIS data, over TRMM data, however, is very significant and of evident relevance for identifying areas where drought remedial interventions are most needed. Moreover, while seasonal forecast of precipitation is still a demanding challenge, the calculation of fAPAR anomalies is represented as a smooth function of time (Fig. 12), which may help for an easier prediction of trends and anomalies at different moments through the growing season.

4. Discussion

4.1. Large area mapping of climate-soil-vegetation complexes

The map of soil-climate-vegetation complexes (isogrowth zones) is a new type of map focusing on phytophenology and including for each class (complex) associations of different vegetation types, which revealed over a period of 9 years, a similar growing pattern of vegetation as well as a similar leaf display structure. Each class includes a similar dynamics of vegetation response to climatic, soil and anthropogenic factors. Then, a straightforward

comparison of the isogrowth zones map with other vegetation maps such as the one by White [72] and that of the Budyko aridity index shows, obviously, some differences.

It should be noted that the main mapping units in the White map represent climax vegetation of different regions of endemism [72]. In this case, the vegetation complexes used in this context, are usually rather broad, including large geographical locations and several lithological classes, under climatic conditions that are also broadly defined.

The images of Fourier coefficients and associated statistics indicate that this new approach is very well suited to study phenology of terrestrial vegetation over large areas. Moreover the approach is useful considering that temporal phenomena, such as the seasonality of the vegetation, can be displayed and understood in terms of 4 or 5 images instead of a large number (i.e. 108 AVHRR-NDVI images used in the Southern Africa and South America case-studies and more than 250 MODIS-FAPAR images used in the China case study). Therefore, the temporal behavior of vegetation communities occurring over many growing seasons may be summarized in a way that is potentially less cumbersome than other approaches [73].

The advantage of this approach in analyzing multi-temporal NDVI images may extend beyond the mere description and the summarization of foliar rhythms observed at regional scale. For example, the 9 years amplitude image, which appears to relate to interannual variability of leaf display, may serve as a measure of resilience, an important functional response of vegetation to climatic change [39]. In particular areas of high amplitude at low frequencies (i.e. those with periods of 9 and 4.5 years), such as Acacia woodland- bushland of the Kalahari (classes 1 and 4 in Fig. 5), would suggest greater resilience to heightened climatic variation predicted for southern Africa under greenhouse warming scenarios [74]. Conversely, zones where the low frequency components showed small amplitudes, such as the miombo woodlands (classes 13, 16 and 17 in Fig. 5), would tend to indicate a vegetation highly resistant to climatic changes. Of the two types of occurrences, it is likely that communities able to adjust leaf display rapidly in response to changes in available resources (i.e. resilient forms) will be privileged under conditions of heightened climatic variations.

4.2. Response of vegetation phenology to climate variability

The case-study carried out in Europe and North Africa covered just three years, which is too short period of time for drawing generic conclusions on the response of foliar phenology to interannual climate variability. On the other hand, in that case, a strong correlation has been found between the Fourier

coefficients and the ratio of precipitation over net radiation. (The inverse of the Budyko ratio has been applied for the study on Europe, where wetter climatic conditions are occurring in comparison with those ones in Southern Africa and South America). In this context, among the amplitude and phase coefficients, the mean NDVI and the 1-year amplitude were the most sensitive indicators of vegetation response to climate variability.

The sensitivity of the Fourier amplitude and phase coefficients to climate variability was evaluated both in the time and spatial domain. In both cases the sensitivity decreased with increasing wetness (i.e. P / R_n). When considering changes in the spatial domain, the sensitivity S of mean NDVI becomes negligible at $P / R_n \approx 1.5$, while the S value for the 1-year amplitude becomes negligible at $P / R_n \approx 2.5$.

It is worth noting that negative S -values were obtained for the 1-year amplitude at $P / R_n \approx 0.5$, i.e. that the 1-year amplitude decreases with the increasing of wetness. This apparently contradictory result can be explained by considering that under semi-arid conditions, an increase in rainfall may increase minimum NDVI more than the maximum NDVI during the year, thus leading to smaller 1-year amplitudes.

4.3. Early detection of anomalies in vegetation conditions

An early information on impending drought may be confirmed by concurrent observations of multiple land surface state variables, such as the Land Surface Temperature (LST) in addition to fAPAR. For the Sichuan and Chongqing case-study the LST anomaly anticipated the appearance of the fAPAR anomaly by a few weeks, and it remained smaller throughout all the period between end of April 2006 and end of August 2006. On the other hand, the LST anomaly, once appeared, it was always evident, thus providing an additional and crucial information on the impending drought event, well in advance on the time of peak-severity (August 2006).

In practice, both fAPAR and LST measures seem to respond consistently to climate forcing. An evaluation of fAPAR and LST response to rainfall, estimated with TRMM data, was performed by Jia and Bastiaanssen [62]. Although the large difference in spatial and temporal resolution between rainfall (TRMM) and fAPAR (MODIS) observations does not allow an accurate comparison, it is clear that the observed fAPAR anomalies respond rather well and correctly to the observed rainfall. The latter supports the use of fAPAR observations for detecting and forecasting drought-related anomalies in vegetation growth. Finally, the advantage of detecting anomalies and drought trends in the Sichuan and Chongqing case-study by means of measures both of water availability and response of terrestrial vegetation, consisted in the

capability of monitoring the beginning of drought occurrence 2 months before the anomaly events reached their peaks (late August).

5. Conclusions

The review presented here illustrates the results obtained over about 20 years by applying time series analysis techniques to extract concise information from extended time series of large area multispectral satellite data. Selected parameters obtained by FFT and HANTS analyses i.e. the 1-year, 6-months and the 9-years amplitudes as well as the 6-months phase images are closely related to the distribution of vegetation types and can be applied for image classifications based on temporal dynamics of the vegetation at regional and continental level. Overall, aridity represents a strong determinant of both vegetation type and of vegetation phenology, which concept is largely supported by the detailed correlation analysis between Fourier coefficients and Budyko index. In particular, the highest correlation coefficients were obtained for the 1-year and 6-months amplitude values. This information, supported by the close match between the White [72] vegetation map and the map of isogrowth zones, indicates the importance of aridity, as measured by the Budyko ratio (B) [31], in determining both phenology and vegetation type.

This conclusion is further supported by the fact that the map of isogrowth zones was obtained through a two-steps classification procedure, where, first, classes have been defined by using an unsupervised classification algorithm to define signatures from Fourier coefficients then other related procedures were applied to obtain the isogrowth map. This implies that each class of the isogrowth map shows similar phenology as measured by the Fourier coefficients. Finally, the correlation of Fourier coefficients with B provides further evidence that small changes in aridity are able to determine subtle differences in vegetation types and, particularly, in the association of vegetation species.

The dependence of the NDVI Fourier spectra on climate variability in time and space has been established quantitatively. Such correlation was stronger in the spatial domain than in the temporal domain, suggesting that the Fourier spectra can be used as a measure of resilience of vegetation to interannual climate variability. Only under very dry conditions interannual climate variability has a larger impact on phenology than spatial variability in dryness. The results on quasi-real-time monitoring and early warning of droughts are preliminary and much remains to be done on issues such as filtering and gap-filling of time series as well as on the accurate and timely detection of anomalies. The review presented here, however, shows that the information on vegetation physiognomy and dynamics obtained by multi-spectral data

collected by imaging radiometers is very reliable and relationships robust over a range of space and time scales.

The results summarized and reviewed here open a two-fold perspective for further research:

1. The abundance of spaceborne observations of the global land surface which span 25 years or more, has a climatological relevance far superior to what was achievable with the data available 20 years ago when this research began. Therefore, this invaluable source of information deserves the most urgent attention, by a deeper and more robust understanding of the observed response of the terrestrial biosphere to climate variability and, specifically, to inter-annual variability;
2. both methods and data have become ripe enough to develop further an efficient and cost-effective early warning system for drought events, based directly on observations of vegetation conditions from space.

References

1. Menenti, M., Bastiaanssen, W.G.M., Hefny, K., Abd El Karim, M.H., 1991, *Report 43. DLO Winand Staring Centre, Wageningen, The Netherlands*, 116.
2. Menenti, M., Azzali, S., Verhoef, W., van Swol, R., 1993, *Adv. Space Res.*, 13(5), 233.
3. Goward, S.N., Tucker, C.J., Dye, D.G., 1985, *Vegetatio*, 64, 31.
4. Townshend, J.R.G., Justice, C.O., 1986, *Int. J. Rem. Sens.*, 7(11), 1435.
5. Justice, C.O., Townshend, J.R.G., Holben, B.N., Tucker, C.J., 1985, *Int. J. Rem. Sens.*, 6(8), 1271.
6. Justice, C.O., Hiernaux, P.H.Y., 1986, *Int. J. Rem. Sens.*, 7, 1475.
7. Justice, C.O., Holben, B.N., Gwynne, M.D., 1986, *Int. J. Rem. Sens.*, 7(11), 1453.
8. Potter, C.S., Brooks, V., 1998, *Int. J. Rem. Sens.*, 19, 2921.
9. Henricksen, B.L., Durkin, J.W., 1986, *Int. J. Rem. Sens.*, 7(11), 15831.
10. Hielkema, J.U., Prince, S.D., Astle, W.L., 1986, *Int. J. Rem. Sens.*, 7, 1499.
11. Malo, A.R., Nicholson, S.E., 1990, *J. Arid Environments*, 19, 1.
12. Anyamba, A., Tucker, C.J., 2005, *J. Arid Environments*, 63, 596.
13. Justice, C.O., Dugdale, G., Townshend, J.R.G., Narracott, A.S., Kumar, M., 1991, *Int. J. Rem. Sens.*, 12, 1349.
14. Henricksen, B.L., 1986, *Int. J. Rem. Sens.*, 7, 1447.
15. Tucker, C.J., Justice, C.O., Prince, S.D., 1986, *Int. J. Rem. Sens.*, 7, 1571.
16. Tucker, C.J., Fung, I.Y., Keeling, C.D., Gammon, R.H., 1986, *Nature*, 319, 195.
17. Liu, W.T., Negrón Juárez, R.I., 2001, *Int. J. Rem. Sens.*, 22, 3483.
18. Seiler, R.A., Kogan, F., 2002, *Adv. Space Res.*, 30, 2489.
19. Gurgel, H.C., Ferreira, N.J., 2003, *Int. J. Rem. Sens.*, 24, 3595.
20. Poveda, G., Salazar, L.F., 2004, *Rem. Sens. Environ.*, 93, 391.
21. Azzali, S., Menenti, M., 1999, *Int. J. Appl. Earth Observation and Geo-information*, 1, 9.

22. Azzali, S., Menenti, M., 2000, *Int. J. Rem. Sens.*, 21 (5), 973.
23. González-Loyarte, M. M., Menenti, M., Di Blasi, A. M., 2008, *Int. J. Climatol.*, DOI: 10.1002/joc.1610.
24. Bolle, H. J., Eckardt, M., Koslowsky, D., Maselli, F., Melia-Miralles, J., Menenti, M., Olesen, F.S., Petkov, L., Rasool, I., Van de Griend, A., 2006. In: "Mediterranean land-surface processes assessed from space". Springer, Berlin.
25. Verhoef, W., Menenti, M., Azzali, S., 1996, *Int. J. Rem. Sens.*, 17, 231.
26. Roerink, G.J., Menenti, M., Verhoef, W., 2000, *Int. J. Rem. Sens.*, 21 (9), 1911.
27. Jia, L., Menenti, M., 2000, *Adv. Earth Sciences*, 21(21), 1254.
28. González-Loyarte, M. M., Menenti, M., 2008, *Int. J. Rem. Sens.*, 29 (4), 1125.
29. Budyko, M. I., 1958. The Heat Balance of the Earth's Surface, trs. Nina A. Stepanova, US Department of Commerce, Washington, D.C., 259.
30. Budyko, M.I., 1974, *Climate and life*. Academic Press, New York, 508.
31. Henning, D., Flohn, H., 1977, Climate aridity index map. In: Explanatory note of United Nations Conference on Desertification, 7.
32. Fuller, D.O., Prince, S.D., 1996. In: Azzali, S., Menenti, M., (Eds). Fourier Analysis of Temporal NDVI in the Southern African and American Continents, *Winand Staring Centre for Integrated Land, Soil and Water Research. Wageningen, the Netherlands. Report 108*, 114.
33. Menenti, M., Azzali, S., Verhoef, W., 1995, Zwerver, S. et al. (eds.), *Climate change research: evaluation and policy implications*, Elsevier, Amsterdam, 425.
34. Roerink, G.J., Menenti, M., Soepboer, W., Su, Z., 2003, *Phys. Chem. Earth.*, 28, 103.
35. Reichle, D.E., ed., 1973, *Analysis of temperate forest ecosystems*, Ecological studies, 1. Springer-Verlag, New York.
36. Lugo, A., 1974, Farnworth, E.G., Golley, F.B., (Eds.), *Fragile ecosystems*. Springer Verlag, New York, 67.
37. Aber, J.D., Melillo, J.M., 1991, *Terrestrial ecosystems*, Saunders College Pub., 427.
38. Swanson, F.J., Wondzell, S.M., Grant, G.E., 1992, Hansen, A.J., di Castri, F. (eds.), *Ecological Studies nr.92*, Springer-Verlag, New York, USA, 304.
39. Walker, B.H., 1993, *Ambio*, 22, 2-3, 80.
40. Turner, B.L. II, Meyer, W.B., Skole, D.L., 1994, *Ambio*, 23-1, 91.
41. Gosz, J.R., 1991, In: Holland, M.M., Risser, P.G., Naiman, R.J.(eds), *Ecotones: the role of landscape boundaries in the management and restoration of changing environment*, Chapman & Hall, London, England, 8
42. Johnson, L.B., 1990, *Landscape Ecology*, 4, 1, 31.
43. Delcourt, P.A., Delcourt, H.R. 1992, In: Hansen, A.J., di Castri, F. (eds.), *Ecological Studies nr.92*, Springer-Verlag, New York, USA, 19.
44. Neilson, R.P., 1986, *Science*, 232, 27.
45. Neilson, R.P., 1987, *Vegetatio*, 70, 135.
46. Leith, H. (ed.), 1974, *Phenology and seasonality modeling*. Springer-Verlag, New York, USA.
47. Reed, B.C., Brown, J.F., Vanderzee, D., Loveland, T.R., Merchant, J.W., Ohlen, D.O., 1994, *J. Veg. Sc.*, 5, 703.
48. Justice, C.O., (ed.); 1986, *Int. J. Rem. Sens.*, 7, 11, 1383.
49. Lloyd, D., 1990, *Int. J. Rem. Sens.*, 12: 2269.

50. Turcotte, K.M, Lulla, K., Venugopal, G., 1993, *Geocarto International*, 4 , 73.
51. Running, S.W., Loveland, T.R., Pierce, L.L., 1994, *Ambio*, 23, 1, 77.
52. Eidenschink, J.C., Haas, R.H., 1992, *Geocarto International*, 1, 53.
53. Eastman J.R., Fulk, M., 1993, *Phot. Eng. & Rem. Sens.*, 59, 6, 991.
54. Lambin E.F., Strahler, A.H., 1993, *Rem. Sens. Environ.*, 48, 231.
55. Viovy, N., Saint, G., 1994, *IEEE Trans. Geoscience and Rem. Sens*, 32-4 : 906.
56. Olsson, L., Eklundh, L., 1994, *Int. J. Rem. Sens.*, 5, 18, 3735.
57. Tau, J.T., Gonzalez, R.C., 1974. Pattern recognition principles, Applied mathematics and computation, n.7. Addison-Wesley, 377.
58. D'Urso G., Menenti, M., 1996, *ISPRS J. Photog. Rem. Sens.*, 51, 2, 78.
59. Ayala, R.M., Menenti, M., 2001, Teledetección, Medio Ambiente y Cambio Global, 469.
60. Azzali, S., Menenti, M., 1996 (Eds). Fourier Analysis of Temporal NDVI in the Southern African and American Continents, *Winand Staring Centre for Integrated Land, Soil and Water Research. Wageningen, the Netherlands. Report 108*, 151.
61. Myneni, R.B., Knyazikhin, Y., Zhang, Y., Tian, Y., Wang, Y., Lotsch, A., Privette, J.L., Morisette, J.T., Running, S.W., Nemani, R., Glassy, J., Votava, P., 1999, MODIS leaf area index (LAI) and fraction of photosynthetically active radiation absorbed by vegetation (FPAR) product (MOD15) Algorithm Theoretical Basis Document, Version 4.0.
62. Jia, L., Bastiaanssen, W.G.M., 2007, Cost-Benefit Analysis: China Drought Monitoring and Prediction Tool. A brief case study of the 2006 Sichuan Drought. Report of Preparatory Study. Alterra, Wageningen University and Research Centre, 31.
63. Fourier, J., 1818, *Bulletin des Sciences par la Société Philomatique*, 126.
64. Box, G.E.P., Jenkins, G.M., 1970, Time series analysis, forecasting and control. Holden Day, San Francisco, Ca., USA.
65. Brandt, S., Damen, H.D., 1989, Quantum Mechanics on the Personal Computer, Springer Verlag, Berlin, Heidelberg, Germany.
66. Main, I.G., 1990, Vibrations and Waves in Physics. Cambridge Univ. Press.
67. Holben, B.N., 1986, *Int. J. Rem. Sens.*, 7, 1435.
68. Los, S.O., 1993, *Int. J. Rem. Sens.*, 14, 10, 1907.
69. Dunn, J.C., 1973, *J. Cybern*, 3, 32.
70. Bezdek, J.C., Ehrlich, R., Full, W., 1984, *Computer & Geosciences*, 10, 191.
71. Kent, J.T., Mardia, K.V., 1988, *IEEE Trans. on PAMI*, 10, 5, 659.
72. White, F., 1983, The vegetation of Africa: a descriptive memoir to accompany the UNESCO/AETFAT/ UNSO vegetation of Africa, *Natural Resources Research*, 20, UNESCO, Paris, 356.
73. Malingreau, J.P., 1986, *Int. J. Rem. Sens.*, 7, 9, 1121.
74. Pittock, A.B., Salinger, M.J., 1991, *Climatic Change*, 18, 205.